Available online at www.sciencedirect.com
ScienceDirect
Journal of Colloid and Interface Science 311 (2007) 417–424
JOURNAL OF Colloid and Interface Science
www.elsevier.com/locate/jcis

Synthesis and size control of monodisperse copper nanoparticles by polyol method

Bong Kyun Park [a], Sunho Jeong [a], Dongjo Kim [a], Jooho Moon [a,*], Soonkwon Lim [b], Jang Sub Kim [b]

[a] *Department of Materials Science and Engineering, Yonsei University, Seoul 120-749, South Korea*
[b] *LCD R&D Center, Samsung Electronics Co. Ltd., Gyeonggi-Do 449-711, South Korea*

Received 25 November 2006; accepted 17 March 2007

Available online 24 March 2007

Abstract

We describe herein the synthesis of metallic copper nanoparticles in the presence of poly(vinylpyrrolidone), employed as a protecting agent, via a polyol method in ambient atmosphere. The obtained copper particles were confirmed by XRD to be crystalline copper with a face-centered cubic (fcc) structure. We observed monodisperse spherical copper nanoparticles with a diameter range 45 ± 8 nm. The particle size and its distribution are controlled by varying the synthesis parameters such as the reducing agent concentration, reaction temperature, and precursor injection rate. The precursor injection rate plays an important role in controlling the size of the copper nanoparticles. On the basis of XPS and HRTEM results, we demonstrate that the surface of the copper is surrounded by amorphous CuO and that poly(vinylpyrrolidone) is chemisorbed on the copper surface.

Keywords: Cu nanoparticles; Polyol synthesis; Particle size control; Surface characterization; Conductive ink

1. Introduction

During the last two decades, a substantial body of research has been directed toward the synthesis of metal nanoparticles in efforts to explore their special properties and potential applications [1–4]. Among various metal particles, copper nanoparticles have attracted considerable attention because of their catalytic, optical, and electrical conducting properties [5–8]. Copper nanoparticles are particularly attractive for application in printed circuit boards (PCBs) and flexible electronics.

Metal nanopowders can be used as a key constituent for preparing the paste or ink from which conductive tracks are patterned by either screen printing or ink-jet printing. The melting point (T_m) of nanomaterials can be dramatically lowered by decreasing the size of the material relative to their bulk counterparts [9]. This low temperature melting ability makes metal nanopowders potentially suitable materials for use in printed electronics, since they can be annealed at lower temperatures to form conductive films of low resistance.

Currently, mainly noble metals such as gold and silver are being exploited, despite their costliness. In this regard, copper is a good alternative material as it is highly conductive and much more economical than Au and Ag. Several methods have been developed for the preparation of copper nanoparticles, including thermal reduction [5], sono-chemical reduction [5,10], metal vapor synthesis [6], chemical reduction [7], vacuum vapor deposition [8], radiation methods [11], microemulsion techniques [12–14], and laser ablation [15].

Most of the aforementioned methods utilize an oxygen-free environment to synthesize copper as it readily oxidizes in air. Lisiecki et al. [16] prepared copper nanoparticles in an aqueous solution using sodium dodecyl sulfate as capping molecules. They employed a glove box to prevent oxidation of the particles. Joshi et al. and Wu et al. independently reported the synthesis of copper nanoparticles in an aqueous system under a nitrogen atmosphere [10,17]. Unlike to other techniques, in the present study, we have developed a polyol method for the preparation of highly monodisperse copper nanoparticles in air. Use of nonaqueous solvent as a reaction medium allows us to minimize the copper surface oxidation. Furthermore, poly(vinylpyrrolidone) added as a dispersing agent also effectively prevents the oxidation process. A key advantage of polyol

* Corresponding author. Fax: +82 2 365 5882.
E-mail address: jmoon@yonsei.ac.kr (J. Moon).

0021-9797/$ – see front matter
doi:10.1016/j.jcis.2007.03.039

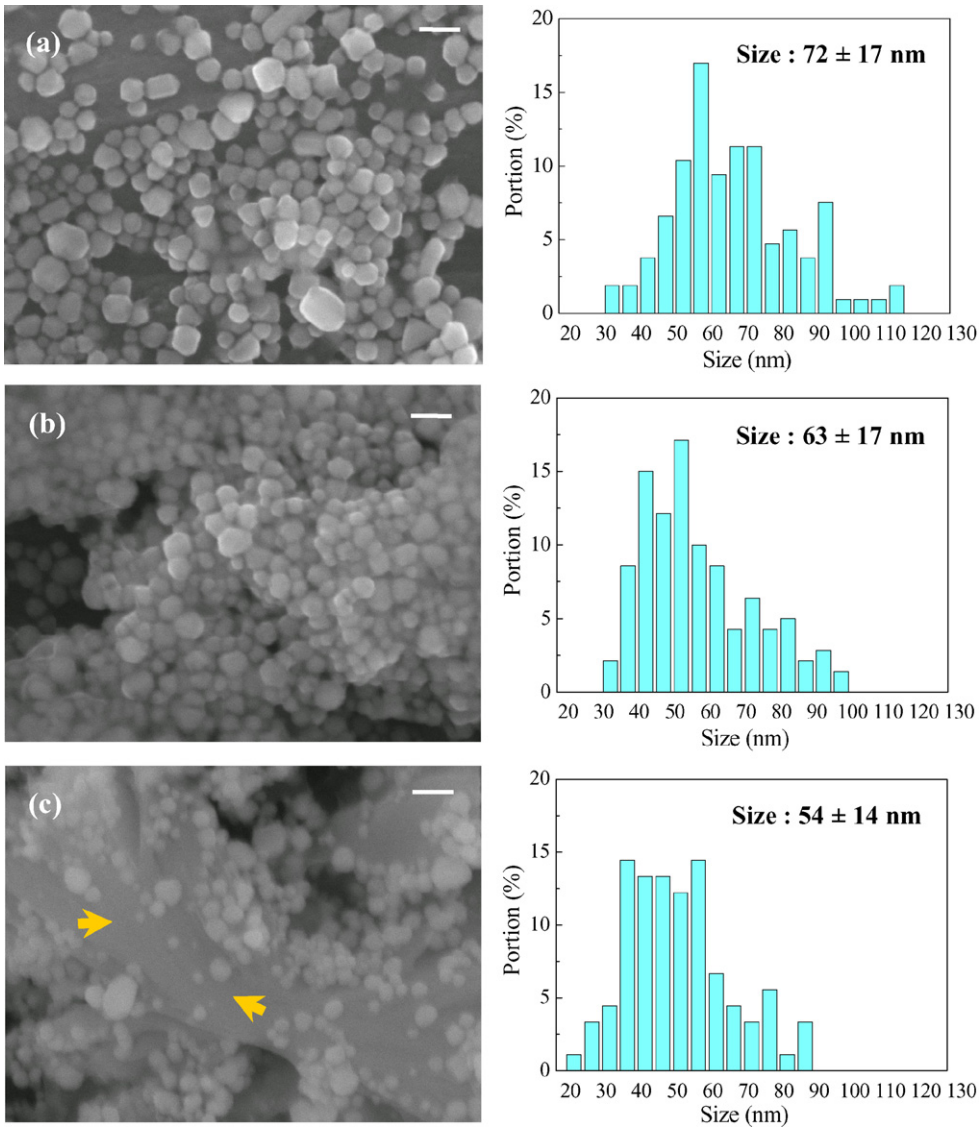

Fig. 1. SEM images and particle size distribution of synthesized copper particles as a function of the amount of reducing agent: (a) 12.75 mmol (sample #1); (b) 17.53 mmol (sample #2); and (c) 19.13 mmol (sample #3). Scale bar = 100 nm. The arrows represent an impurity phase.

process-based nanoparticle synthesis is that the reaction kinetics can be easily controlled, as demonstrated by Fievet et al. [18–21]. We have controlled the size and size distribution of the particles by varying experimental parameters such as the amount of reducing agent, reaction temperature, and precursor injection rate.

2. Experimental

2.1. Preparation of copper particles

Poly(*N*-vinylpyrrolidone) (PVP, M_w = 40,000, Sigma–Aldrich), acting as a capping molecule, was dissolved in diethyleneglycol (DEG, 99%, Sigma–Aldrich). Sodium phosphinate monohydrate ($NaH_2{\cdot}PO_2{\cdot}H_2O$, Junsei), used as a reducing agent, was added to the DEG solution and the solution was heated to reaction temperatures. The aqueous solution of copper(II) sulfate pentahydrate (98%, Sigma–Aldrich) was then injected into the hot reaction medium via a syringe pump. The injection rate of the Cu salt solution was varied from 2 to 8 ml/min. After 1 h of reaction, the solution was cooled to room temperature and the particles were separated by centrifugation and then washed with methanol. The detailed reaction conditions employed in the particle synthesis are summarized in Table 1.

2.2. Characterization

Phase composition and crystallinity of the synthesized copper particles were investigated using an X-ray diffractometer (XRD, DMAX2500, Rigaku) employing Cu$K\alpha_1$ radiation (1.51059 Å). The morphology of the copper particles was investigated via scanning electron microscopy (SEM, JSM-6500F, JEOL) and the particle size distributions were obtained by image analysis. The surface compositions of the copper particles were investigated by X-ray photoelectron spectroscopy (XPS, ESCALAB 22i-XL, VG Scientific Instrument) and the sur-

Table 1
Synthesis conditions for the preparation of copper particles using the injection method

Sample ID	Reducing agent (mmol)	Reaction temperature (°C)	Injection rate (ml/min)	Cu salt (mmol)
#1	12.75	200	2	20
#2	17.53	200	2	20
#3	19.13	200	2	20
#4	17.53	200	8	20
#5	17.53	170	8	20
#6	17.53	140	8	20
#7	17.53	200	6	20
#8	17.53	140	2	80
#9	17.53	140	6	80
#10	17.53	140	8	80

face morphology was examined by high resolution transmission electron microscopy (HRTEM, JEM-4010, JEOL).

3. Results and discussion

3.1. Influence of reducing agent

In a typical polyol process, a polyol liquid such as diethyleneglycol acts not only as a reaction medium but also as a reducing agent. However, in the case of copper nanoparticle synthesis, the reducing ability of diethyleneglycol is insufficient to reduce the copper ions because copper is easily oxidized to either CuO or Cu_2O in air atmosphere [22]. We introduce $NaH_2PO_2{\cdot}H_2O$ as a reducing agent. $NaH_2PO_2{\cdot}H_2O$ is generally used in aqueous chemical reduction for the preparation of copper particles. It produces oxidation reaction represented by the equation

$$H_2PO_2^- + H_2O \rightarrow H_2PO_3^- + 2H^+ + 2e^-, \quad (1)$$

in an acidic condition, releasing electrons. The released electrons are utilized to reduce copper ions as shown in the equation

$$Cu^{2+} + 2e^- \rightarrow Cu. \quad (2)$$

According to the equations, the rate and amount of the electrons supplied to the copper ions are determined by sodium phosphinate. In this study, we control the synthesis reaction kinetics by adjusting the amount of the reduction agent.

Fig. 1 shows SEM images of particles synthesized with varying amounts of reducing agent. At low reducing agent concentration (12.75 mmol), the reducing rate of the copper precursor is sluggish and consequently only a few nuclei are formed at the nucleation step. Precipitating copper atoms at the later period of the reaction are mostly involved in particle growth by collision with already generated nuclei rather than in the formation of new particles. This reaction mechanism leads to the formation of larger sized particles, as shown in Fig. 1a. With increasing reducing agent concentration, the enhanced reduction rate favors the generation of more nuclei, resulting in the formation of smaller copper particles (Fig. 1b). At a higher reduction rate (19.13 mmol), the number of precipitating metallic clusters steeply increases and considerably more nuclei are produced during a single event of the nucleation period. Eventually, the size of particles decreases because the amount of

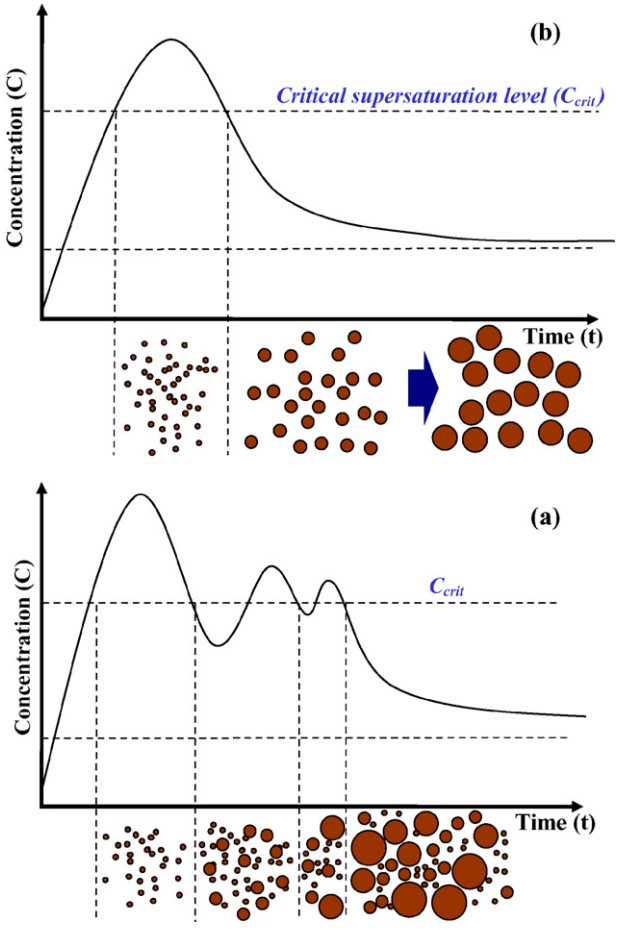

Fig. 2. Schematic illustration of nucleation and growth mechanisms based on LaMer's model: (a) mechanism for polydisperse particles and (b) mechanism for monodisperse particles.

solute available for particle growth per growing particle decreases with the increasing number of nuclei. The reaction at higher reducing agent concentration also leads to the formation of an unidentified impurity phase, as shown in Fig. 1c. In a polyol process, the dissolved metal ions are not directly reduced into a neutral metal species, but transformed into an intermediate solid phase comprised of hydroxyethyleneglycolate or corresponding alkoxide radicals prior to nucleation step. Then, the re-dissolved metal ion from the intermediate solid phase is consumed in nucleation and growth processes [23,24]. In this regard, it is considered that the intermediate solid phase itself is reduced in the presence of extremely high reducing agent, forming unidentified impurity phase.

The particle characteristics of the synthesized copper are determined by the nucleation and growth mechanisms. When the reduction rate of copper ions exceeds the consumption rate of copper clusters by particle growth, the concentration of reduced copper atoms (C) likely remains over a critical supersaturation level (C_{crit}) for longer time or fluctuates around C_{crit}. This allows an extended nucleation period or multiple nucleation events and, in turn, the growing period of each nucleus will differ (Fig. 2a). Therefore, the final particles exhibit broader size compared to that of particles grown at the same rate after a single nucleation event (Fig. 2b).

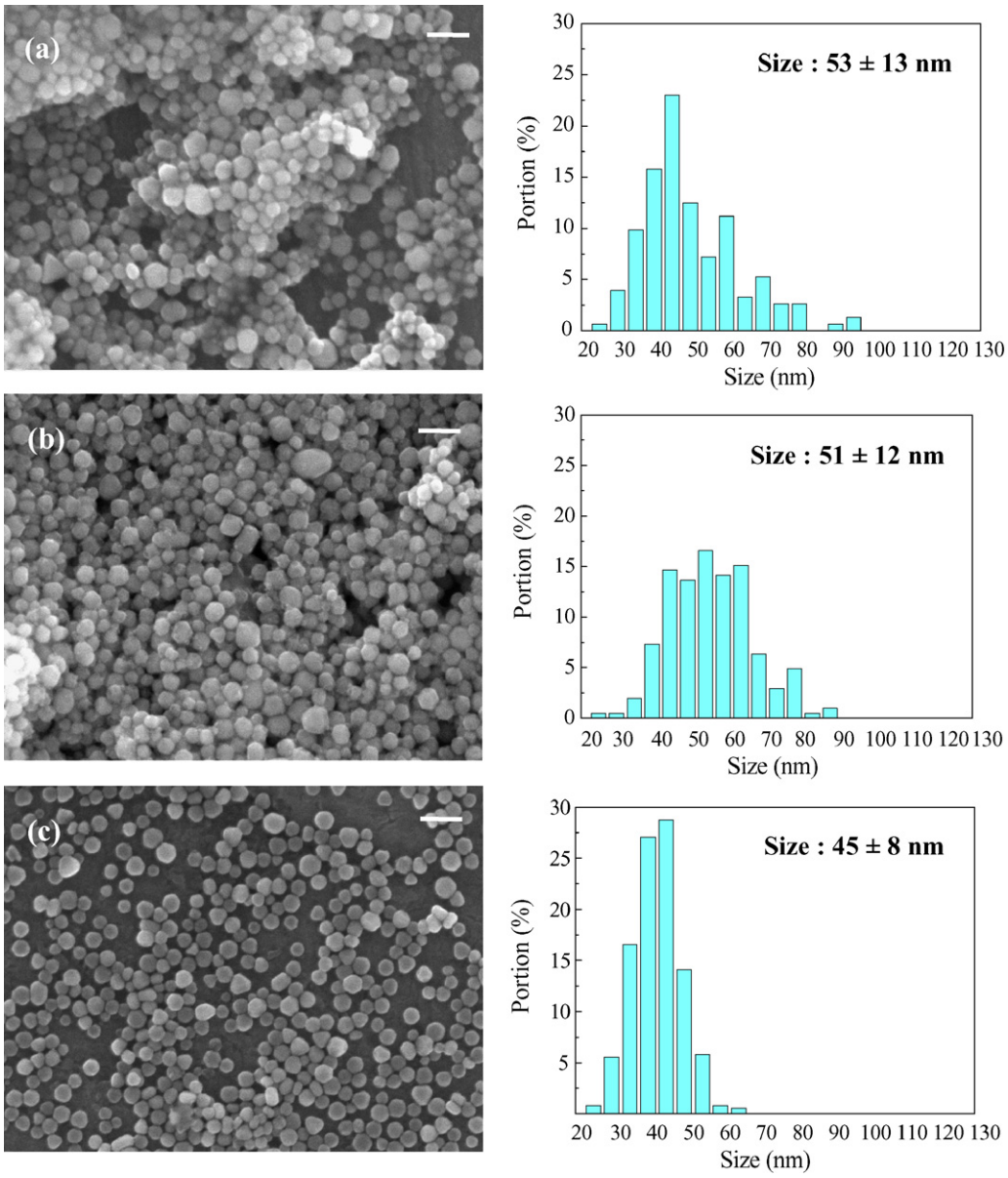

Fig. 3. SEM images and particle size distribution of synthesized copper particles as a function of the reaction temperature: (a) 200 °C (sample #4); (b) 170 °C (sample #5); and (c) 140 °C (sample #6). Scale bar = 100 nm.

3.2. *Influence of reacting temperature*

Fig. 3 shows SEM images of copper particles synthesized at different temperatures. With decreasing reaction temperature, the size of the resulting particles becomes smaller and the size distribution is also narrowed. At 200 °C, the obtained particle size was 53 ± 13 nm (Fig. 3a), whereas that at the synthesis temperature of 140 °C was 45 ± 8 nm (Fig. 3c). When copper salt solution is injected into a reaction medium maintained at 200 °C, the color of the medium in the vicinity where the precursor solution is added changes from light yellow to dark red. This indicates that copper particles are rapidly generated when the precursor solution is injected. A high reducing rate at the temperature of 200 °C allows instantaneous multiple nucleations to occur when the precursor solution is added dropwise. The resulting particles at this condition exhibit a relatively broad size distribution due to uneven particle growth and coagulation of the primary particles.

In contrast to the reaction at 170 and 200 °C, the color of the reaction medium changes to light blue rather than dark red when the precursor solution is injected at 140 °C. The aqueous solution of copper ions has a blue color. This indicates that there is no immediate reduction of copper ions upon addition to the reaction medium. After approximately 10 s, the solution suddenly turns dark red, indicating nucleation. If the number of nuclei is large enough to lower the concentration of copper atoms below the critical supersaturation level, no further nucleation occurs and the nucleated particles continue to grow. Coagulation of the primary particles would be unlikely because the thermal energy is not sufficient for vigorous particle movement. Under these nucleation and growth conditions, as depicted in Fig. 2b, the resulting particles are relatively monodisperse. At

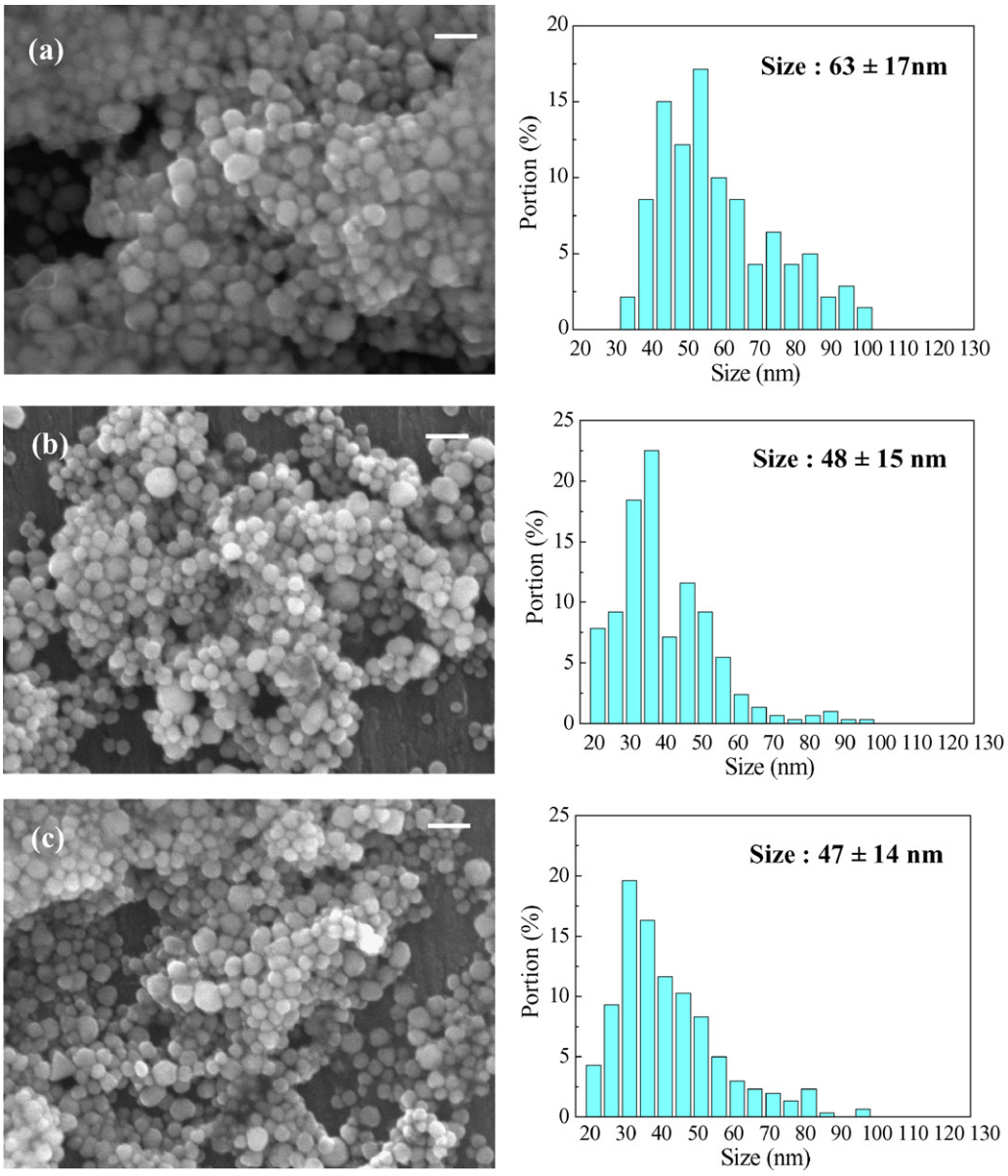

Fig. 4. SEM images and particle size distribution of copper particles synthesized at 200 °C as a function of the precursor injection rate: (a) 2 ml/min (sample #2); (b) 6 ml/min (sample #7); and (c) 8 ml/min (sample #4). Scale bar = 100 nm.

temperature lower than 140 °C, however, the reaction medium remains light blue in color, implying that the copper ions do not undergo reduction to copper atoms.

3.3. *Influence of injection rate*

We also controlled the injection rate of the copper salt precursor to the PVP dissolved polyol medium. Fig. 4 shows SEM images of particles with synthesized different precursor injection rates at 200 °C. The particles become smaller and narrower as the injection rate is increased. At an injection rate of 2 ml/min, the obtained particle size was 63 ± 17 nm (Fig. 4a), whereas that at 8 ml/min was 47 ± 14 nm (Fig. 4c). The injection rate determines the amount of copper ions per unit time to be reduced. When the reduction rate is high enough to reduce copper ions as soon as they are supplied, the precursor injection rate will be equal to the production rate of copper atoms. The concentration of copper atoms slowly reaches C_{crit} at slow injection of the precursor. The nucleation rate is sluggish and the number of nuclei is small. Therefore, the resulting particles are large and broad. In contrast, fast injection of the precursor results in a steep increase in the concentration of copper atoms, permitting a short burst of nucleation and generating many nuclei. This leads to smaller particles with better monodispersity.

The influence of the precursor injection rate varies depending upon the reaction temperature. Fig. 5 shows SEM images of particles synthesized with different precursor injection rates at 140 °C. Contrary to the previous results, the particles tend to become larger and broader as the injection rate is increased. At 2 ml/min, the obtained particle size was 60 ± 10 nm (Fig. 5a) whereas that at 8 ml/min was 68 ± 20 nm (Fig. 5c). If the reac-

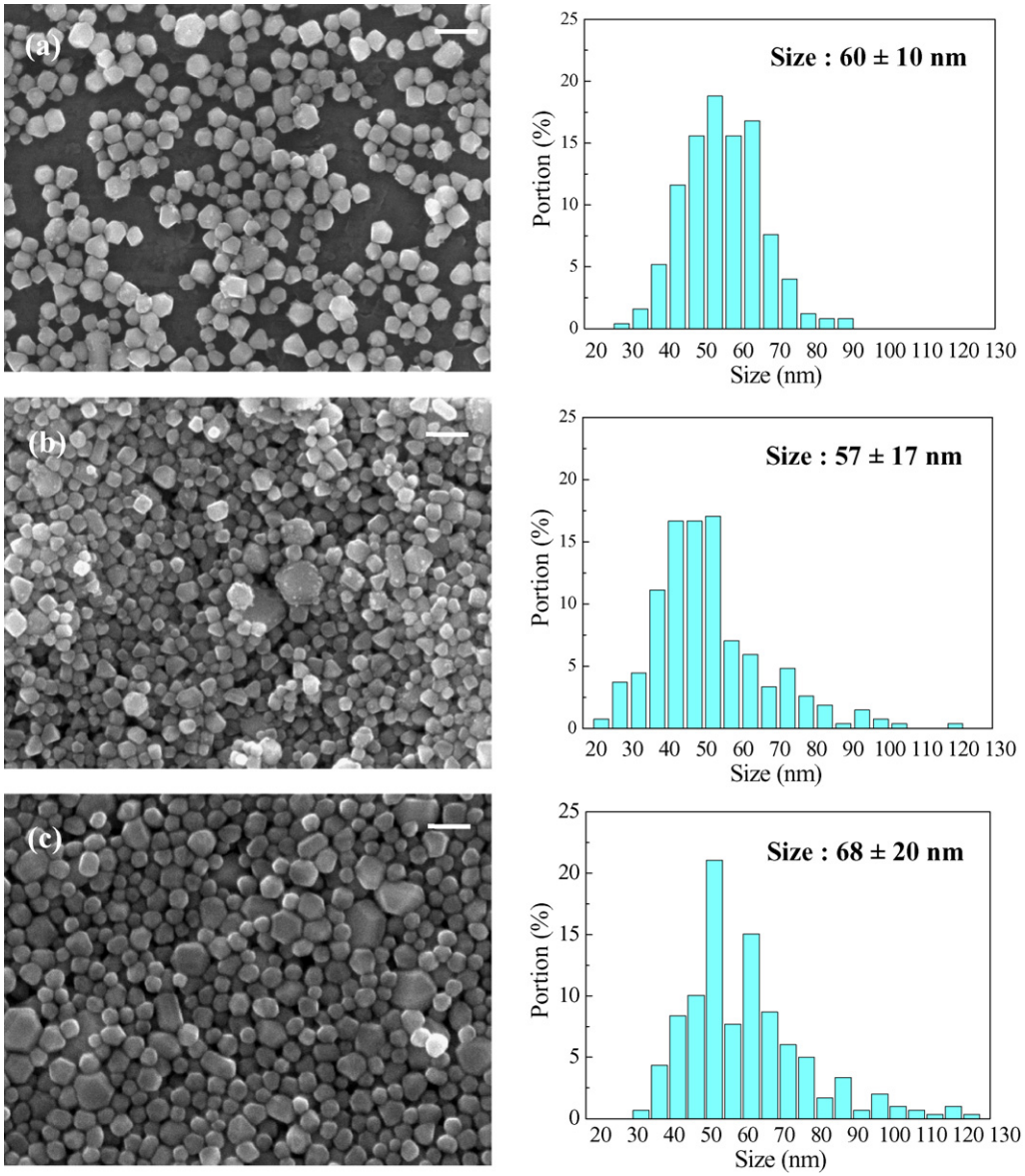

Fig. 5. SEM images and particle size distribution of copper particles synthesized at 140 °C as a function of the precursor injection rate: (a) 2 ml/min (sample #8); (b) 6 ml/min (sample #9); and (c) 8 ml/min (sample #10). Scale bar = 100 nm.

tion rate is too fast at lower temperature, the generation rate of copper atoms exceeds the rate of consumption of copper atoms by particle growth and multiple nucleations may occur, resulting in polydisperse particles.

3.4. Characteristics of copper particles

In addition to particle size and distribution, particle characteristics were also investigated. Monodisperse Cu particles (sample #6) were used for the phase and surface composition analyses. The particles synthesized in ambient atmosphere were determined to be phase-pure Cu without any impurity phase such as CuO, Cu_2O, or $Cu(OH)_2$. X-ray diffraction patterns correspond to crystalline copper characteristic peaks with a face-centered-cubic (fcc) crystal structure as shown in Fig. 6. The same X-ray diffraction peaks were observed for the sample stored for 30 days in ambient condition.

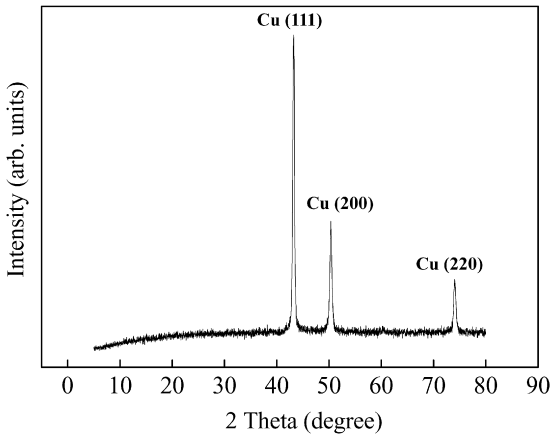

Fig. 6. X-ray diffraction pattern of copper particles synthesized at 140 °C with an injection rate of 8 ml/min (sample #6).

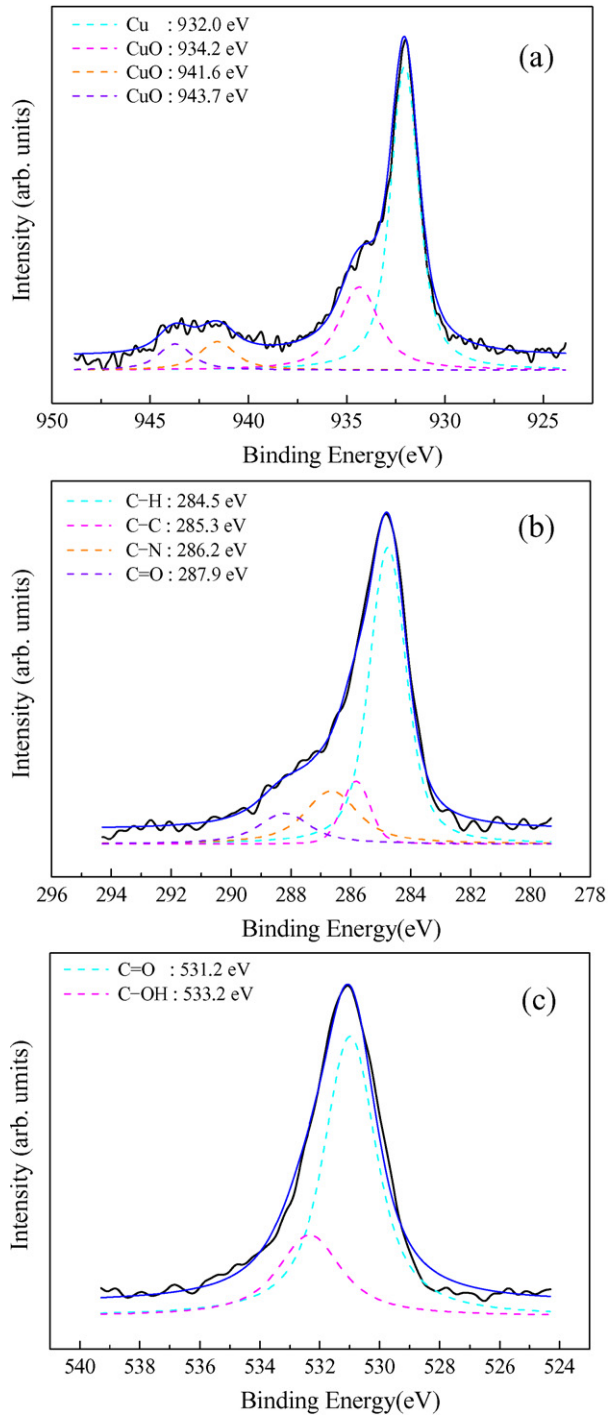

Fig. 7. X-ray photoelectron spectra of Cu nanoparticles: the peaks from (a) Cu $2p_{3/2}$, (b) C 1s, and (c) O 1s.

Surfaces of copper particles are analyzed by X-ray photoelectron spectroscopy (XPS) as shown in Fig. 7. We identified a copper peak at 932.0 eV together with weak CuO peaks at 934.2 eV, as shown in Fig. 7a [23]. The existence of PVP is also confirmed by XPS spectra of C 1s. The C 1s spectrum is composed of four peaks and the binding energies of these peaks are 284.5 eV (C–H bonding), 285.3 eV (C–C bonding), 286.2 eV (C–N bonding), and 287.9 eV (C=O bonding). These binding energies can be attributed to four types of carbon atoms in PVP.

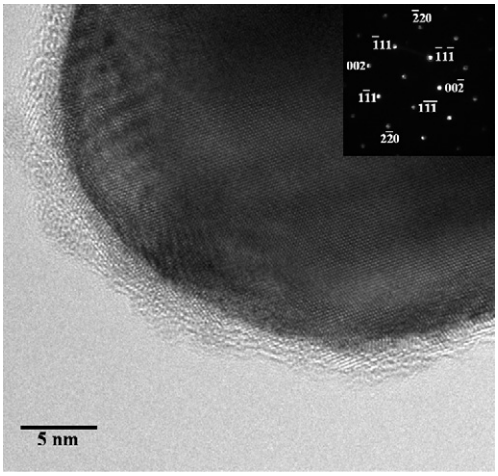

Fig. 8. HRTEM image of the synthesized Cu nanoparticles. The inset is the selected area diffraction pattern.

The O 1s peak composed of two peaks, one placed at 531.2 eV (C=O bonding) and the other placed at 533.2 eV (C–OH bonding). The O 1s peak from the carboxyl (C=O) oxygen atom at 531.2 eV shifts to higher binding energy relative to pure PVP, indicating that the PVP is strongly chemisorbed to the surface of copper particles [24]. This interaction is achieved by coordination bond between Cu ions and PVP molecules, and Cu ions are surrounded by PVP molecules prior to nucleation step [25–27]. Thus, the chemically adsorbed PVP molecules can prevent the copper particles from oxidation during the nucleation and growth processes. However, incomplete prevention from the oxidation takes place. The oxidation has two main origins. The Cu nanoparticles were synthesized from water containing polyol medium in ambient condition. Some oxygen dissolved in the reaction medium results in partial oxidation at the surface of the Cu nanoparticles. Some oxidation may also occur when the samples for analysis are prepared in air.

Fig. 8 shows an HRTEM image of the synthesized Cu particles. Most of the particles are single crystals, but some contain a twin boundary. The surface of the particle is surrounded by an amorphous layer with a thickness of ∼1.5 nm. All the selected area diffraction patterns correspond to face-centered-cubic structured Cu, showing no crystalline CuO. Based on the XPS and HRTEM results, it appears that the surface amorphous layer consists of chemisorbed PVP and amorphous CuO.

4. Conclusions

We have synthesized copper nanoparticles in ambient atmosphere by a polyol method. The obtained copper particles were confirmed to be phase-pure crystalline copper with face-centered cubic (fcc) structure on the basis of XRD analyses. Detailed surface analyses by XPS and HRTEM revealed that the synthesized particles consist of single crystal Cu surrounded by amorphous CuO and chemisorbed PVP with a thickness of ∼1.5 nm. We have adjusted the synthesis parameters to control the size and size distribution of the particles. Particle size decreases with increasing reducing agent concentration. The Cu precursor injection rate plays an important role in controlling

the particle size, whereas reaction temperature determines the particle size distribution. We obtained relatively monodisperse copper nanoparticles with a size range of 45 ± 8 nm at optimum conditions.

Acknowledgments

This work was supported by the Korea Science and Engineering Foundation (KOSEF) through the National Research Lab. Program funded by the Ministry of Science and Technology (No. M10500000011).

References

[1] G.G. Ferrier, A.R. Berzins, N.M. Davey, Platinum Metals Rev. 29 (1985) 175.
[2] J.H. Fendler, Chem. Rev. 87 (1987) 877.
[3] N. Toshima, T. Yonezawa, New J. Chem. 22 (1998) 1179.
[4] M. Brust, C.J. Kiely, Colloids Surf. A 202 (2002) 175.
[5] N.A. Dhas, C.P. Raj, A. Gedanken, Chem. Mater. 10 (1998) 1446.
[6] G. Vitulli, M. Bernini, S. Bertozzi, E. Pitzalis, P. Salvadori, S. Coluccia, G. Martra, Chem. Mater. 14 (2002) 1183.
[7] H.H. Huang, F.Q. Yan, Y.M. Kek, C.H. Chew, G.Q. Xu, W. Ji, P.S. Oh, S.H. Tang, Langmuir 13 (1997) 172.
[8] Z. Liu, Y. Bando, Adv. Mater. 15 (2003) 303.
[9] D. Kim, S. Jeong, J. Moon, Nanotechnology 17 (2006) 4019.
[10] R.V. Kumar, Y. Mastai, Y. Diamant, A. Gedanken, J. Mater. Chem. 11 (2001) 1209.
[11] I.G. Casella, T.R.I. Cataldi, A. Guerrieri, E. Desimoni, Anal. Chim. Acta 335 (1996) 217.
[12] I. Lisiecki, M.P. Pileni, J. Am. Chem. Soc. 115 (1993) 3887.
[13] M.P. Pileni, B.W. Ninham, T. Gulik-Krzywicki, J. Tanori, I. Lisiecki, A. Filankembo, Adv. Mater. 11 (1999) 1358.
[14] L. Qi, J. Ma, J. Shen, J. Colloid Interface Sci. 186 (1997) 498.
[15] M.S. Yeh, Y.S. Yang, Y.P. Lee, H.F. Lee, Y.H. Yeh, C.S. Yeh, J. Phys. Chem. B 103 (1999) 6851.
[16] I. Lisiecki, F. Billoudet, M.P. Pileni, J. Phys. Chem. 100 (1996) 4160.
[17] S. Wu, D. Chen, J. Colloid Interface Sci. 273 (2004) 165.
[18] G. Viau, F. Fievet-Vincent, F. Fievet, Solid State Ionics 84 (1996) 259.
[19] P.Y. Silvert, K. Tekaia-Elhsissen, Solid State Ionics 82 (1995) 53.
[20] F. Fitvet, J.P. Lagier, B. Blin, B. Beaudoin, M. Figlarz, Solid State Ionics 32–33 (1989) 198.
[21] F. Fievet, F. Fievet-Vincent, J.P. Lagier, B. Dumont, M. Figlarz, J. Mater. Chem. 3 (1993) 627.
[22] R.A. Swalin, Thermodynamics of Solid, second ed., Wiley, New York, 1972, p. 114.
[23] M. Yin, C.K. Wu, K. Lou, C. Burda, J.T. Koberstein, Y. Zhu, S. O'Brien, J. Am. Chem. Soc. 127 (2005) 9506.
[24] P. Jiang, S.Y. Li, S.S. Xie, Y. Gao, L. Song, Chem. Eur. J. 10 (2004) 4817.
[25] Y. Gao, P. Jiang, D.F. Liu, H.J. Yuan, X.Q. Yan, Z.P. Zhou, J.X. Wang, L. Song, L.F. Liu, J.M. Zhang, D.Y. Shen, J. Phys. Chem. B 108 (2004) 12877.
[26] B. Yin, H. Ma, S. Wang, S. Chen, J. Phys. Chem. B 107 (2003) 8898.
[27] I. Washio, Y. Xiong, Y. Yin, Y. Xia, Adv. Mater. 18 (2006) 1745.